Structure of liquid Ga and the liquid-vapor interface of Ga

Meishan Zhao, Dmitriy S. Chekmarev, Zhong-Hou Cai, and Stuart A. Rice
Department of Chemistry and The James Franck Institute, The University of Chicago, Chicago, Illinois 60637
(Received 2 June 1997)

This paper describes a quantitative comparison of the predicted and observed structure in the liquid-vapor interface of a metal. We report the results of a theoretical study of the structure of the liquid-vapor interface of Ga, based on self-consistent quantum Monte Carlo simulations using a pseudopotential representation of the electron-ion and the ion-ion interactions. The single-particle density distribution along the normal to the interface is predicted to display stratification, with a spacing of about an atomic diameter and the amplitude of the density oscillations decaying to zero after about a four-layer penetration into the bulk liquid. The pair structure function in the plane of the liquid-vapor interface is predicted to be essentially the same as that in the bulk liquid. The qualitative and quantitative character of these predictions are in very good agreement with the results of recent experimental studies. [S1063-651X(97)08912-5]

PACS number(s): 68.10.−m

I. INTRODUCTION

The difference between the structure of the liquid-vapor interface of a simple dielectric liquid, such as Ar, and that of a simple liquid metal, such as Cs, can be interpreted as a consequence of the way spheres pack in the different effective fields in the two interfaces [1–4]. The key elements in this interpretation are the realization that a gradient in the single-particle density along the normal to the interface, which we call the longitudinal density distribution, is supported by a one-body effective force acting on the molecules in the interface and that that force can, in dielectrics and metals, vary slowly or rapidly on the scale of the molecular diameter. In the case of a dielectric, the effective intermolecular pair potential is, to a very good approximation, independent of the molecular density, so does not vary across the liquid-vapor interface; the one particle force that arises from the variation of the average energy per molecule with density varies slowly across that interface. It then follows that the liquid-vapor interface will have the monotone longitudinal density distribution characteristic of the packing of spheres in a slowly varying external potential. In contrast, in the case of a liquid metal the effective ion-ion potential is strongly electronic density dependent. It is found [5–15] that in this case the energy per ion varies very rapidly across the liquid-vapor transition zone, generating a strong short-ranged one-particle retaining force. Consequently, the longitudinal density distribution is characteristic of the packing of spheres in a strongly varying external potential, e.g., like the oscillatory density distribution of a hard-sphere liquid adjacent to a smooth hard wall. The qualitative features of the longitudinal density distributions in the liquid-vapor interfaces of dielectrics and metals have been confirmed experimentally. This paper is concerned with a quantitative comparison of the predicted and observed structure of the liquid-vapor interface of Ga.

The prediction that the liquid-vapor interface of a metal is stratified for several layers was made by D'Evelyn and Rice [6–8], for Na and Hg, based on self-consistent quantum Monte Carlo simulations using the pseudopotential representation of the ion-ion and electron-ion interactions. Subsequent calculations led to similar predictions for the longitudinal density distributions in the liquid-vapor interfaces of Cs and Mg and showed that the predicted stratification is robust with respect to many features of the pseudopotential employed. Although there was experimental evidence that provided weak confirmation of the general character of the predicted longitudinal density distribution in the liquid-vapor interface of a metal [16] as early as 1984, strong evidence for the predicted behavior of that distribution was provided by Pershan and co-workers [17–20] from x-ray reflectivity studies of Ga and Hg. One of the major purposes of this paper is to use these recently obtained data to provide a quantitative test of the accuracy of the theoretical approach of Rice and co-workers [5–15,21,22] by a comparison of the predicted and observed structure of the liquid-vapor interface of Ga.

The pioneering simulation of the structure of the liquid-vapor interface of Hg, by D'Evelyn and Rice [6–8], was based on the study of a small free cluster of atoms and a local electroneutrality approximation. These investigators also used a semiempirical ansatz to allow for a metal-to-nonmetal transition in the inhomogeneous liquid-vapor transition region. Because of the use of these approximations and the very small size of the simulation sample, we believe the results of the D'Evelyn-Rice calculations can only provide a qualitative or semiquantitative description of the structure of the liquid-vapor interface of Hg.

The approximations originally used by D'Evelyn and Rice were removed in later theoretical developments by Rice and co-workers [9–15]. Once a particular form for the pseudopotential is accepted, the self-consistent quantum Monte Carlo simulation provides the exact Born-Oppenheimer level representation of the electron and ion density distributions in the liquid-vapor interface of the metal. Of course, the representations of the pseudopotential and its rate of change with electron density incorporate approximations, so the results of the computer simulations must be tested against experimental data to verify the accuracy of those approximations. Prior to the work reported in this paper, the most accurate prediction of the structure of the liquid-vapor interface of a metal concerned Cs. By use of the words ''most accurate'' we mean that the pseudopotential

representation of the properties of alkali metals has been sufficiently tested against the properties of the solid and liquid phases of these elements that one can have considerable confidence in the quality of the representation. However, there are no experimental data yet available concerning the character of the longitudinal and transverse atomic distributions in the liquid-vapor interface of Cs or any other alkali metal. When, in 1989, Ga became a vehicle of choice for the experimental study of the liquid-vapor interface of a metal, we initiated a parallel theoretical study. That study has proved to be very challenging because of the complex character of liquid Ga.

Most metals have both a crystal structure and a liquid structure determined primarily by the constraints defining the packing of spheres at the appropriate density, and for most metals, as for most of the dielectrics, the crystalline phase is denser than the liquid phase. These simple rules do not apply to Ga. The structure of crystalline Ga just below the melting point at 29.78 °C is very different from that of other metals; the unit cell, which is orthorhombic with lattice constants $a = 4.5103$ Å, $b = 4.4861$ Å, and $c = 7.6463$ Å, contains eight atoms [23,24]. The atoms are paired so as to form psudodiatomic molecules in the sense that each Ga atom has one very close neighbor at 2.44 Å and six other neighbors, themselves paired as in diatomic molecules, at distances ranging from 2.71 to 2.79 Å. The pseudodiatomic molecules are arranged in planes. It has been argued that this crystal structure is consistent with the properties of the Ga electron-ion pseudopotential [25]. The argument makes use of the distribution of locations in reciprocal lattice space of the Brillouin zone planes that just bound the Fermi sphere, relative to the location of the smallest-wave-number zero of the part of the pseudopotential that represents the energy of the electron gas in the crystal potential; these relative locations are so distributed that there is destabilization of the symmetric face-centered-cubic (fcc), body-centered-cubic (bcc), and hexagonal-close-packed (hcp) lattices relative to the observed lattice structure. Similarly, the structure function of liquid Ga differs from that characteristic of simple liquid metals, such as Na and Cs, in having a prominent shoulder on the high-wave-number side of the first peak [26–28]. There is a corresponding asymmetry in the shape of the first peak of the pair-correlation function. It is argued by some [29] that the shoulder in the first peak of the structure function is an averaged response to the same feature in the Ga pseudopotential that leads to the complicated atomic packing in the crystalline state. It is argued by others [30] that the anomaly in the structure of liquid Ga is associated with a change in the curvature of the effective pair potential in the vicinity of the near-neighbor separation; a symmetric first peak in the pair-correlation function is attributed, by these investigators, to monotone curvature of the effective pair potential in the vicinity of the near-neighbor separation.

We also note that, since liquid Ga is denser than crystalline Ga, the density in the liquid-vapor transition zone must at some point have the same value as in the solid. Given that the structure of solid Ga clearly displays pseudodimerization of atoms and anisotropic ordering of the pseudodimers, and given the interpretation of the shoulder in the structure factor of liquid Ga as the response to the same forces that define the unusual crystal structure, the longitudinal and transverse atomic distributions in the liquid-vapor interface of Ga could differ somewhat from those of simple metal for which the liquid is less dense than the solid [31]. The results of our calculations show that the predicted longitudinal and transverse density distributions in the liquid-vapor interface of Ga are similar to those for other metals; we also show that these distributions are in excellent agreement with the available experimental data.

II. OVERVIEW OF THE METHOD OF CALCULATION

As in our previous work [5–15], the analysis of the structure of the liquid-vapor interface of Ga reported in this paper is based on the pseudopotential theory of metals. In this theory the interaction between the delocalized electrons and the ions is represented by a nonlocal potential that takes account of the requirement that the states of the delocalized electrons are orthogonal to the states of the core electrons. For convenience in the calculations of the energy of the metal, it is a common practice to first model the positive ion distribution as a ''jellium'' (with a defined liquid-vapor density profile) in which free electrons move and then to account for the effects associated with the discrete nature of the positive ions by use of second-order perturbation theory. In this representation the Hamiltonian of the liquid metal with N ions is given by

$$H=\sum_{i=1}^{N}\left[\frac{p_i^2}{2m}+\sum_{j<i}\phi_{\rm eff}(R;n_e(\mathbf{r}))\right]+U_0(\rho_0(\mathbf{r}),n_e(\mathbf{r})), \tag{2.1}$$

where $\mathbf{p}_i$ is the momentum of ion i with mass m, $R=|\mathbf{R}_i-\mathbf{R}_j|$ is the distance between ion cores i and j, $\mathbf{r}$ is a point in the system at which the electronic density is $n_e(\mathbf{r})$ and the ion density is $\rho_0(\mathbf{r})$, $\phi_{\rm eff}(R;n_e(\mathbf{r}))$ is the effective interaction potential between ions i and j, and $U_0(\rho_0(\mathbf{r}),n_e(\mathbf{r}))$ is the so-called structure-independent part of the potential energy. We note that $U_0(\rho_0(\mathbf{r}),n_e(\mathbf{r}))$ is a functional of the ion density distribution, which, in this representation, contains the electronic kinetic energy, the electrostatic energy of the system, the exchange-correlation energy, and the first-order perturbation theory contribution to the energy from the electron-discrete ion pseudopotential.

The effective ion-ion interaction potential $\phi_{\rm eff}(R;n_e(\mathbf{r}))$ can be shown to have two components, namely, the screened direct interaction between ions with effective valence z^* and the indirect interaction, the so-called band structure energy, which arises from the second-order term in the perturbation theory representation of the electron-ion pseudopotential. In a homogeneous fluid with electronic density $n_e(\mathbf{r})$ this effective potential is given by

$$\phi_{\rm eff}(R)=\frac{(z^*)^2}{R}\left\{1-\frac{2}{\pi}\int_0^\infty\frac{F_N(q)\sin(qR)}{q}\,dq\right\}+W(R). \tag{2.2}$$

In Eq. (2.2), $F_N(q)$ is the normalized energy wave-number characteristic function, which depends on the atomic volume of the metal but not on the structure of the liquid, and $W(R)$ is the contribution to the energy arising from the core polar-

ization and the core-core repulsion. We note that $W(R)$ is usually small relative to the other contributions to the energy.

We have used the expression

$$F_N(q)=\frac{\Omega^2 q^4}{16\pi^2(z^*)^2}\left\{\frac{[1-\varepsilon(q)](v_1+v_2)^2}{\varepsilon(q)} +2g(q)(v_1+v_2)+\varepsilon(q)[g(q)]^2+h(q)\right\}, \tag{2.3}$$

due to Shaw [32], to calculate $F_N(q)$. In Eq. (2.3), Ω is the atomic volume, $\varepsilon(q)$ is the wave-number-dependent Hartree dielectric function, $g(q)$ is the nonlocal screening function, $h(q)$ is a nonlocal bare pseudopotential contribution of the second order, and $v_1=-4\pi Z/\Omega q^2$ and $v_2=4\pi\overline{Z}/\Omega q^2$ are the local potential contributions arising from the valence charge Z and the depletion hole charge $\overline{Z}$. The Hartree dielectric function is given by

$$\varepsilon(q)=1+\frac{1}{2\pi k_F\eta^2}\left[1+\frac{1-\eta^2}{2\eta}\ln\left(\left|\frac{1+\eta}{1-\eta}\right|\right)\right], \tag{2.4}$$

with k_F the Fermi wave number and $\eta=q/2k_F$. The nonlocal screening function $g(q)$ is defined as

$$g(q)=\frac{4}{\pi^2 q^2\varepsilon(q)}\int_{k\leqslant k_F}\frac{f(\mathbf{k},\mathbf{q})}{k^2-|\mathbf{k}+\mathbf{q}|^2}\,d\mathbf{k} \tag{2.5}$$

and $h(q)$ as

$$h(q)=\frac{4}{\pi^2 q^2}\int_{k\leqslant k_F}\frac{|f(\mathbf{k},\mathbf{q})|^2}{k^2-|\mathbf{k}+\mathbf{q}|^2}\,d\mathbf{k}, \tag{2.6}$$

while the nonlocal contribution to the bare pseudopotential $V_{\rm ps}^{\rm ion}$ is

$$f(\mathbf{k},\mathbf{q})=-N\langle\mathbf{k}+\mathbf{q}|V_{\rm ps}^{\rm ion}|\mathbf{k}\rangle. \tag{2.7}$$

A more detailed description of the pseudopotential $V_{\rm ps}^{\rm ion}$ will be given in Sec. III.

As already indicated, $U_0(\rho_0(\mathbf{r}),n_e(\mathbf{r}))$ is the sum of the electronic kinetic energy T_e, the electrostatic energy of the system $E_{\rm elec}$, the exchange-correlation energy $E_{\rm xc}$, and the first-order perturbation theory contribution to the energy from the electron-discrete ion pseudopotential $E_{\rm ps}$, i.e.,

$$U_0(\rho_0(\mathbf{r}),n_e(\mathbf{r}))=T_e+E_{\rm elec}+E_{\rm xc}+E_{\rm ps}. \tag{2.8}$$

We have calculated the electronic kinetic energy using a local-density approximation with density gradient corrections. Specifically, we set

$$T_e=E_{\rm FT}+E_W+E_K, \tag{2.9}$$

where

$$E_{\rm FT}=\frac{3(3\pi^2)^{2/3}\sigma}{10}\int_0^\infty dz[n_e(\mathbf{r})]^{5/3} \tag{2.10}$$

is the Fermi-Thomas uniform density approximation to the kinetic energy [33] for a liquid metal with surface area σ,

$$E_W=\frac{\sigma}{72}\int_0^\infty dz\,\frac{|\nabla^2 n_e(\mathbf{r})|}{n_e(\mathbf{r})} \tag{2.11}$$

is the von Weisacker form for the first density correction to the kinetic energy of the inhomogeneous electron gas [34], and

$$E_K=\frac{\sigma}{540(3\pi^2)^{2/3}}\int_0^\infty dz\left\{[n_e(\mathbf{r})]^{1/3}\left[\left(\frac{\nabla^2 n_e(\mathbf{r})}{n_e(\mathbf{r})}\right)^2 -\frac{9}{8}\left(\frac{\nabla^2 n_e(\mathbf{r})}{n_e(\mathbf{r})}\right)\left(\frac{\nabla n_e(\mathbf{r})}{n_e(\mathbf{r})}\right)^2+\frac{1}{3}\left(\frac{\nabla n_e(\mathbf{r})}{n_e(\mathbf{r})}\right)^4\right]\right\}^2 \tag{2.12}$$

is the Kirzhnits form for the second-order gradient correction to the kinetic energy of the inhomogeneous electron gas [35]. The first term in Eq. (2.12) is the linear-response theory contribution to the kinetic energy associated with the fourth-order term in the gradient of the density, while the last two terms are the nonlinear-response contribution to the kinetic energy associated with the gradient of the density. It is understood that the gradient corrections to the electron kinetic energy E_W and E_K are valid in the limit of small gradient in the density of electron gas, i.e., when the electron gas density is slowly varying on the scale of the atomic diameter. From the results of the calculations reported in this paper, we find that this condition is satisfied over most of the liquid-vapor interface of Ga, despite the variation of the ion core density in the interface.

The electrostatic energy of the system, which arises from the difference between the electron and ion density distributions in the liquid-vapor interface transition zone, can be represented in the form

$$E_{\rm elec}=-2\pi\sigma\int_0^\infty dz\int_0^\infty dz'[\rho_0(z)\rho_0(z') -n_e(z)n_e(z')]|z'-z|, \tag{2.13}$$

where $\rho_0(z)$ is the longitudinal ion charge density distribution function and $n_e(z)$ is the longitudinal electron charge density distribution function. We have calculated the exchange-correlation contribution to the energy using the homogeneous electron gas method proposed by Vosko, Wilk, and Nusair [36], with the density gradient correction proposed by Langreth and Mehl [37], i.e.,

$$E_{\rm xc}=2\sigma\int_0^\infty n_e(z)\varepsilon_{\rm xc}(n_e(z))dz, \tag{2.14}$$

where $\varepsilon_{\rm xc}(n_e(z))$ is the integration kernel for the exchange-correlation energy including the gradient corrections. The total contribution of the electron-ion pseudopotential to the electronic energy of the system can be written as

$$E_{\rm ps}=\sigma\int_0^\infty dz\;\rho_0(z)\varepsilon_{\rm ps}(n_e(z)), \tag{2.15}$$

with $\varepsilon_{\rm ps}(n_e(z))$ the ionic pseudopotential function, which is given by

$$\varepsilon_{\rm ps}=\frac{3}{k_F^2}\int_{q\leqslant k_F} f(q,q')q^2dq-\frac{1}{\pi}\int_0^\infty dq\{\rho^2[M(q)]^2 -(z^*)^2F_N(q)\}-\frac{2\pi(z^*)^2}{\Omega}\lim_{q\to 0}\left(\frac{1-F_N(q)}{q^2}\right), \tag{2.16}$$

where $f(q,q')$ is the nonlocal bare electron-ion pseudopotential matrix discussed before and $M(q)$ is the Fourier transform of the depletion hole density.

In order to calculate the energy of an inhomogeneous liquid metal using the representation discussed above we must know both the ionic density and the electronic density distributions as a function of distance normal to the liquid-vapor interface. For the ionic density distribution we adopt the parametric ''jellium'' representation proposed by Rice and co-workers [5–15], namely,

$$\rho(z;z_0,\beta)=\frac{\rho_b}{1+\exp\left\{\dfrac{|z|-z_0}{\beta}\right\}}, \tag{2.17}$$

where z_0 is the position of the surface and ρ_b is the bulk density that is related to z_0 and the parameter β by

$$\rho_b=\frac{N}{2\sigma\left\{z_0+\beta\,\ln\left[1+\exp\left(\dfrac{-z_0}{\beta}\right)\right]\right\}}, \tag{2.18}$$

which guarantees that the liquid density has the bulk value far from the liquid-vapor interface. Usually the Gibbs dividing surface is located at z_0. The density profile parameter β characterizes the rate at which the bulk density falls to the vapor density through the surface transition zone. Both z_0 and β are determined by the ionic configuration. Given Eq. (2.18) for the positive jellium distribution, the electron density distribution can be determined by solving the Kohn-Sham [38] equation, which, for the present case, is identical to the one-dimensional Schrödinger equation

$$\left[-\frac{\hbar^2}{2m}\frac{d^2}{dz^2}+V_{\rm eff}(z)\right]\psi_n(z)=\varepsilon_n\psi_n(z), \tag{2.19}$$

where $V_{\rm eff}(z)$ is an effective potential that includes the interaction of an electron with the ionic background and the exchange-correlation potential. Because the electron density falls to zero rapidly outside the jellium distribution, it is a good approximation to treat the electronic system as bounded in z; this is accomplished by setting $n_e(z)=0$ at a fairly large distance $z=a$ outside the jellium distribution, which in turn is accomplished by including in $V_{\rm eff}(z)$ an infinite hard-wall potential located at $z=\pm(z_0+a)$. The Kohn-Sham equation must be solved self-consistently since the eigenvector sought $\psi_n(z)$ is used in the construction of $V_{\rm eff}(z)$; this process is iterated until convergence is achieved.

All of the preceding refers to the calculation of the electronic energy and the effective ion-ion interaction associated with a particular ionic configuration in the inhomogeneous liquid metal. Of course, in the system of interest to us the ions are mobile and a suitable average over all allowed ionic configurations must be calculated in order to determine the longitudinal and transverse density distributions in the liquid-vapor interface. As will be described below, using the formalism sketched above, an assumed initial jellium distribution is used to generate an electronic density distribution from which the ion-electron pseudopotential and effective ion-ion interaction potentials are calculated. These initial jellium distributions are then used in a Monte Carlo simulation of the inhomogeneous liquid-vapor system. Since each Monte Carlo step changes the ion distribution, it also changes the electronic density distribution and hence the ion-electron pseudopotential and the effective ion-ion interaction; this effect is particularly important in the inhomogeneous liquid-vapor transition zone. Accordingly, when the ion distribution is changed, the electron distribution is recalculated to be consistent with the new ion distribution; this procedure is continued until the Monte Carlo simulation converges.

III. DETAILS OF THE CALCULATIONS

The pseudopotential analysis of the electronic energy of a metal is not unique [39–42]; different choices for the representation of the influence of the core states of the ions lead to different pseudopotentials. For the calculations reported in this paper we employed the energy-independent model pseudopotential proposed by Woo, Wang, and Matsuura [41,42], as successfully applied to the study of simple metals by Harris, Gryko, and Rice. This pseudopotential is given by

$$V_{\rm ps}^{\rm ion}(r)=\sum_l\,[\overline{V_l}(r)+\Delta_l]|l\rangle\langle l|, \tag{3.1}$$

with

$$\Delta_l=[V_{1l}(r)+\overline{V_l}(r)]|R_{1l}\rangle\langle R_{1l}|, \tag{3.2}$$

where $\overline{V_l}(r)$ is an average of the pseudopotential, for each angular momentum l, over all states other than the first valence state, $|R_{1l}\rangle$ is the radial part of the wave function for the state $|1l\rangle$, and $|l\rangle$ is a simple projection onto the state with angular momentum l. For the present calculation the model pseudopotential takes the form

$$V_{1l}(r)=\begin{cases}-B_{1l}+\dfrac{Z_l}{r}, & r<R_l\\[2ex] \dfrac{-Z}{r}, & r<R_l,\end{cases} \tag{3.3}$$

where B_{1l},Z_l,R_l are parameters and Z is the valence of the ion. The state $|1l\rangle$ is separated into radial and angular parts, such that

$$\langle\mathbf{x}|1l\rangle=CR_{1l}(r)Y_{lm}(\theta,\phi), \tag{3.4}$$

where $R_{1l}(r)=r^{-1}y_{1l}(r)$, C is a normalization constant, $Y_{lm}(\theta,\phi)$ is a spherical harmonic function, and the radial part of the wave function is given by the regular and irregular Whittacker functions

TABLE I. Ion pseudopotential parameters (a.u.) for liquid gallium. r_{max} is the maximum value of r in the radial function.

l	E_{1l}	R_l	B_{1l}	r_{max}
0	1.128 602 3	1.941 040	1.546 509	35.0
1	1.105 059 8	0.534 974	4.344 044	45.0
2	0.472 135 7	2.023 584	0.335 127	55.0

$$y_{1l}(r)=\begin{cases} M_{\nu,l+1/2}(2\lambda r), & r<R_l \\ W_{\nu_0,l+1/2}(2\lambda_0 r), & r>R_l. \end{cases} \tag{3.5}$$

The parameters that appear in Eq. (3.5) are related by

$$\begin{aligned} &\lambda_0=(-2E_{1l})^{1/2}, \quad \lambda=[-2(E_{1l}+B_{1l})]^{1/2}, \\ &\nu_0=Z_l/\lambda_0, \qquad\quad \nu=-Z_l/\lambda, \end{aligned} \tag{3.6}$$

with E_{1l} the spectroscopic term energy [43] of the state $|1l\rangle$. We have extracted the values of the other independent parameters pertinent to our calculation from the work of Shaw [40]; the values of these parameters are listed in Table I.

We show in Fig. 1, for homogeneous fluid Ga at several electron densities, the normalized wave-number characteristic function $F_N(q)$. The small ''kink'' near $q=2k_F$, which is found in the corresponding functions for many other liquid metals, is a signal of the logarithmic singularity at $q=2k_F$ in the Hartree static dielectric function.

Figure 2 shows the effective ion-ion pair interaction potential in liquid Ga, calculated using the $F_N(q)$ displayed in Fig. 1. Clearly, the Ga-Ga interaction is rather short ranged, except for the small-amplitude oscillating tail, which is a characteristic feature of the effective ion-ion pair potential in a metal.

The calculations of the effective ion-ion interaction and the energy wave-number characteristic function for Ga displayed in Fig. 1 were carried out for homogenous fluid Ga with different bulk densities. The liquid-vapor interface of the metal is, of course, an inhomogeneous region in which both the electron and ion densities vary with respect to position normal to the liquid-vapor interface. In this paper, as

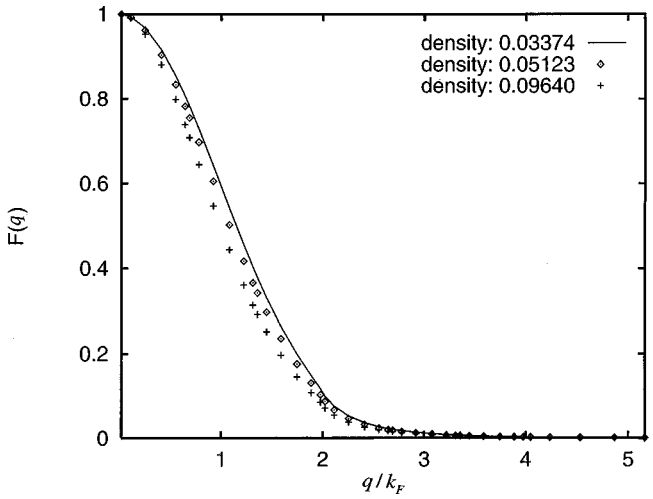

FIG. 1. Normalized wave number characteristic function $F_N(q)$ for liquid Ga at ion densities 0.033 74, 0.051 23, and 0.096 40 atoms/Å^3 [see Eq. (2.3)].

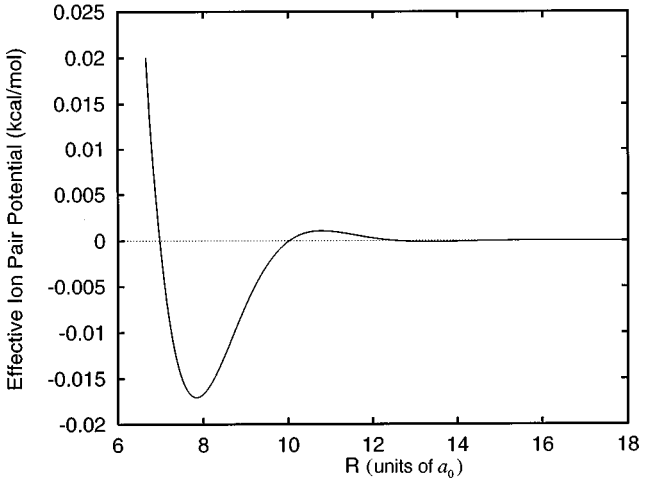

FIG. 2. Effective ion-ion pair interaction potential in liquid Ga calculated from the pseudopotential using the normalized wave number characteristic function $F_N(q)$ displayed in Fig. 1, at a density of 0.051 23 atoms/Å^3. a_0 is the Bohr radius.

in our earlier papers, we have calculated the effective ion-ion interaction in the inhomogeneous liquid-vapor interface using a local-density approximation to the electron density, namely,

$$\phi_{\rm eff}(R)=\phi_H\left(R;\frac{1}{2}[n_e(\mathbf{r}_i)+n_e(\mathbf{r}_j)]\right)\exp\left(-\frac{R}{R_{\rm ion}}\right), \tag{3.7}$$

where $R_{\rm ion}$ is the radius of the Ga pseudoion and the exponential factor is used to account for the effect of mixing of the energy levels of the valence electrons and the electrons in the inner shells.

It is impractical to repeat the calculations of the effective ion-ion interaction for every move of the ions in the Monte Carlo simulation procedure. Before the start of the simulation we computed, for several electron densities ranging from somewhat below to somewhat above the bulk density of liquid Ga, the effective ion-ion interaction potential. During the simulation the interaction between a particular pair of ions was obtained from a rational functional interpolation for the given electron density, using the precalculated data bank.

The model system for the simulations consisted of a slab of 1024 ions and 3072 electrons, with two free surfaces in the positive- and negative-z directions (normal to the two liquid-vapor interfaces) and periodic boundary conditions in the x and y directions. In fact, periodic boundary conditions were also applied in the z direction, but at distances so far from the liquid-vapor interfaces that the description of those interfaces as free is also valid. The dimensions of the simulation slab were $L_0\times L_0\times 2L_0$ in the x, y, and z directions, so that the area of each liquid-vapor interface is $\sigma=L_0\times L_0$. L_0 was chosen such that the average density of ions in the slab matched the density of liquid Ga at the simulation temperature. The center of mass of the simulation system was located at $z=0$ and at the origin of the coordinates. The total depth of the slab was 14 layers (each about an atomic diameter in thickness), so that the depth of one side of the slab was 7 layers. Since the coherence length of the pair correlation function is only of order 3 atomic diameters, this

depth is great enough to ensure that the liquid-vapor interface sits atop bulk liquid Ga. The initial ion configuration was generated by placing the particles at random positions within the boundaries of the slab, subject to the constraint that no ion-ion separation was less than $5a_0$. The trial configurations were generated by randomly displacing a selected ion; the magnitude of the ionic displacement was chosen to lead to convergence to equilibrium with a reasonable overall acceptance ratio for the trial configurations. For each instantaneous ionic configuration we determined the parameters z_0 and β [see Eq. (2.17)], describing the ion distribution along the z direction using the discrete moment method introduced by Harris, Gryko, and Rice [9]. Then, using this jellium distribution, we solved the Kohn-Sham equation and thereby obtained the electron density distribution along the z axis.

For each configuration of the ions the electronic density is a function of z, z_0, and β and the structure independent energy U_0 is a function of β and the liquid bulk density ρ_b. It is convenient to think of U_0 for the inhomogeneous system of interest as the formal sum of the structure-independent energy of a homogeneous system with density ρ_b and the structure-independent, but density-dependent, energy difference between the homogeneous system with density ρ_b and the inhomogeneous system. Then the first term in this formal sum has an invariant value during the Monte Carlo simulation, while the second term gives the surface energy of the reference jellium distribution. It should be noted that z_0 is allowed to vary during the course of the simulation to permit relaxation of the density distribution in the liquid-vapor transition region to its equilibrium form; the variation of z_0 is constrained by the requirement that the center of mass of the slab be invariant. Even with the limited number of ions in our simulation sample, the number of ions in the homogeneous liquid-vapor interface is a very small fraction of the total number of ions, so changes in the interface structure do not affect the ion and electron density distributions in the bulk liquid, with the consequence that the surface energy of the system is a function of the parameter β only.

Prior to starting the Monte Carlo simulation we obtained self-consistent solutions to the Kohn-Sham equation and the electron density distributions for 40 evenly spaced values of β in the range from $\beta=0$ to $1.95a_0$. We show in Fig. 3 the variation of $n_e(z)$ with respect to the change in shape of the positive ion jellium distribution $\rho(z)$. Because the electronic density of liquid Ga is large, even when $\rho(z)$ is discontinuously truncated to form an interface with zero width the Friedel oscillations of the electron density are quite small. As β increases the liquid-vapor interface width increases and the electron longitudinal density distribution approaches the jellium longitudinal density distribution; in the limit that the liquid-vapor interface is very broad the electron and the jellium distributions coincide. The difference between the electron density and jellium density distributions in the liquid-vapor interface is dominated by the competition between achievement of local electroneutrality and avoidance of excess kinetic energy associated with increasing the curvature of the electron wave function.

We show in Fig. 4 the contributions to the surface energy of the Ga liquid-vapor interface, as a function of the interface width parameter β, arising from the kinetic energy, the electrostatic energy, the exchange-correlation energy, and the electron-ion pseudopotential interaction. The surface energy including the pseudopotential contribution is illustrated in Fig. 5, which displays the total surface energy as a function of β. It is the pseudopotential contribution that is responsible for the rapid increase in the surface energy when $\beta>0.4a_0$

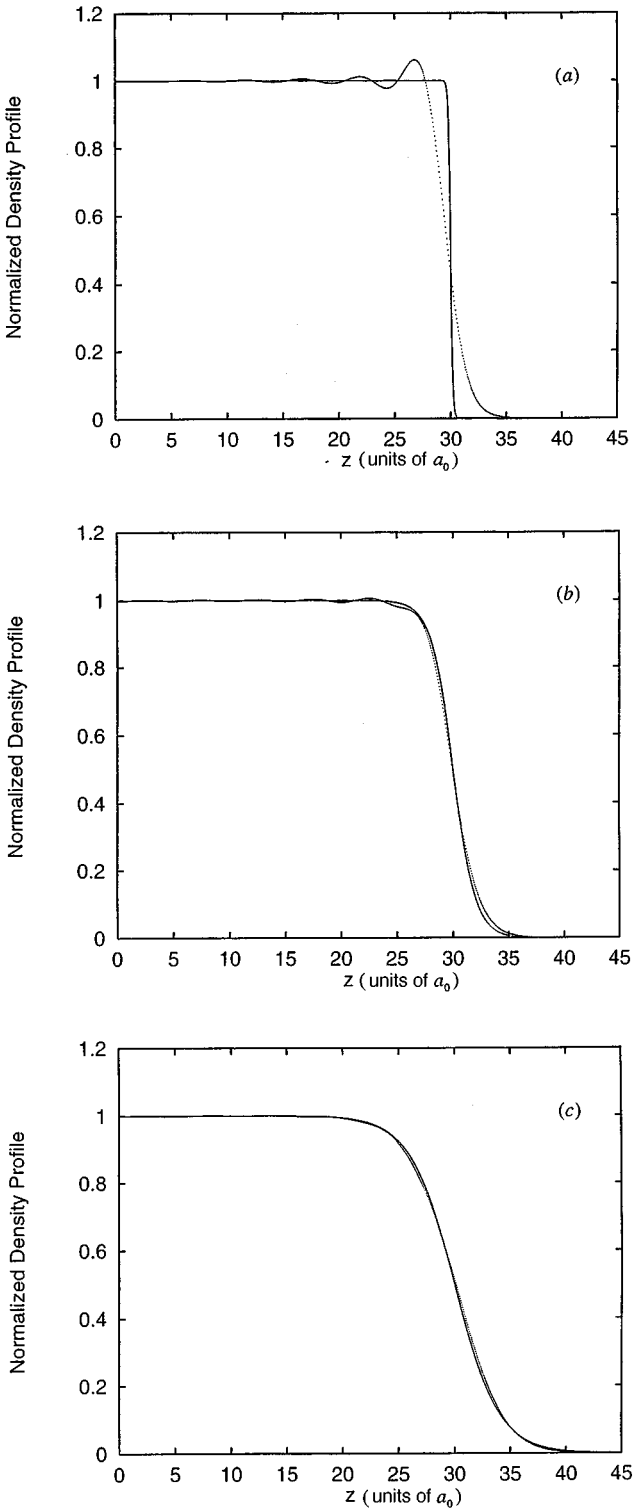

FIG. 3. Normalized longitudinal electronic density profile $n_e(z)/n_{e,\text{bulk}}$ (....) and the normalized jellium longitudinal density distribution $\rho_e(z)/\rho_{\text{bulk}}$ (—): (a) $\beta=0.1a_0$, (b) $\beta=1.0a_0$, and (c) $\beta=2.0a_0$

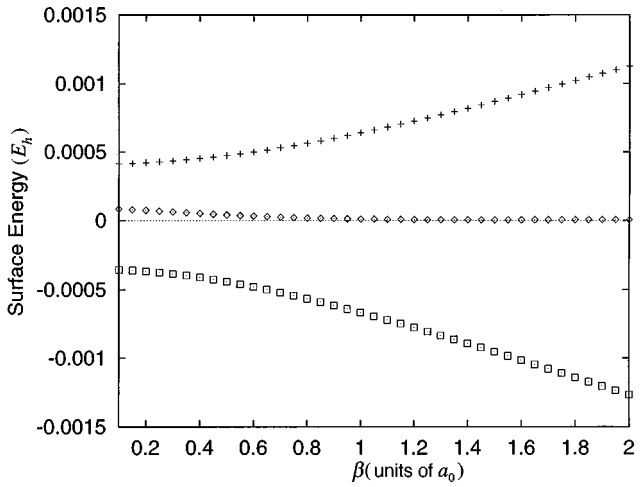

FIG. 4. Contributions to the surface energy as a function of the longitudinal positive ion jellium density width parameter β. From top to bottom: the kinetic energy contribution (+++), the exchange-correlation energy contribution ($\diamond\,\diamond\,\diamond$), and the electrostatic energy contribution ($\square\square\square$).

For convenience, we calculated and tabulated the surface energy as a function of β for the experimental value of the bulk density in order to make a proper comparison of our calculations with experimental data. During the simulation, the surface energy is obtained by interpolation from the set of tabulated values for any desired value of β. In all the calculations reported we have carried out more than 12 000 Monte Carlo passes, with each pass consisting of 1000 ionic configurations. All the results reported in this paper were determined by calculations using the last 8000 passes.

The pair-correlation function in a thin slice parallel to the interface in the x-y plane is calculated from a histogram of the separations of all pairs of particles in that slice. The normalized pair-correlation function is given by

$$g(r)=\left\langle\frac{V_T}{V_S}\right\rangle\left\langle\frac{2N(r,\Delta r)}{N_T^2}\right\rangle, \tag{3.8}$$

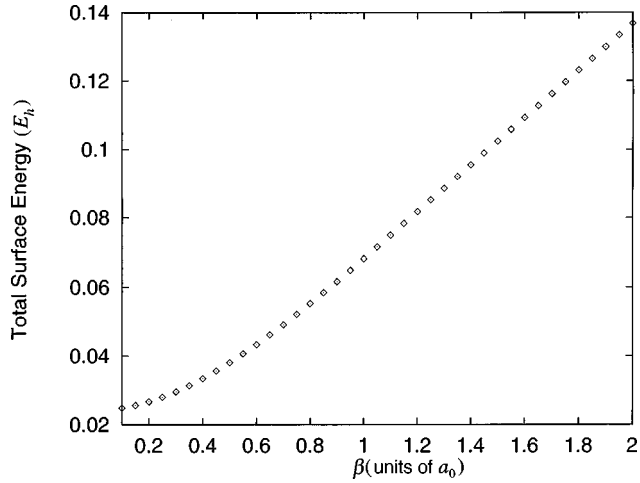

FIG. 5. Total surface energy $U_0(\rho(\vec{r},n_e(\vec{r}))$, as defined in Eq. (1), as a function of the longitudinal positive ion jellium density distribution width parameter β. For a given width parameter β, the densities $\rho(\vec{r})$ and $n_e(\vec{r})$ that appear in $U_0(\rho(\vec{r}),n_e(\vec{r}))$ are those displayed in Fig. 3.

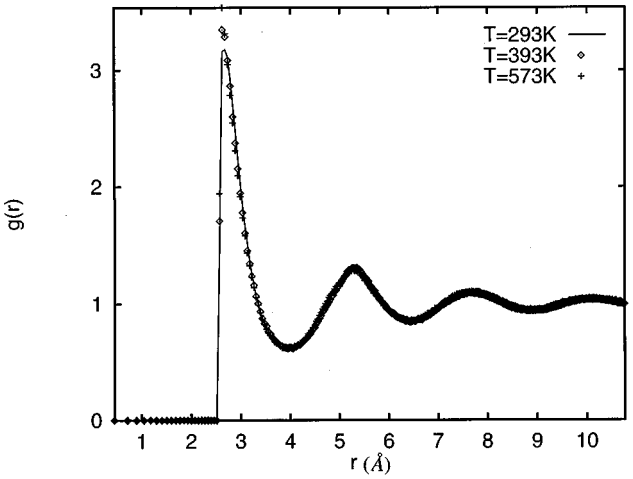

FIG. 6. Pair-correlation functions of bulk liquid Ga at a density 0.051 23 atoms/Å^3 and temperatures $T=273$, 373, and 573 K.

where N_T is the total number of particles in the slice, $N(r,\Delta r)$ is the average number of pairs of particles within a distance between r and $(r+\Delta r)$ in the slice, V_T is the total volume of all the particles in the slice, and V_S is the average volume of the intersection of the spherical shell between r and $(r+\Delta r)$ and the thin slice.

IV. DISCUSSION

Bellissent-Funel, Chieux, Levesque, and Weis, [44] have reported the structure factor of liquid Ga, determined by neutron scattering at $T=326$ and 959 K and densities 0.0525 and 0.0490 atoms/Å^3. Narten [28] has reported the structure factor of liquid Ga, determined from x-ray- and neutron-diffraction data, at $T=293$ K. Since the densities of liquid Ga at 293 and 593 K differ very little, we have compared the results of our calculations with data obtained from both experiments. To illustrate the insignificance of the temperature dependence of the structure factor of liquid Ga in the temperature range mentioned, we have carried out simulations of the pair-correlation function of bulk liquid Ga at various temperatures. These results, which are displayed in Fig. 6, show that the differences between the pair-correlation functions at 293, 393, and 593 K are not observable within the precision of our calculations.

There are three sets of experimental data with which our calculations can be compared.

We show first, in Fig. 7, the calculated and observed pair correlation functions of bulk liquid Ga. We note that the positions of the peaks and troughs of the calculated and measured pair-correlation functions are very nearly the same. Indeed, all the major features of the pair-correlation function of liquid Ga, including the asymmetry in the shape of the first peak and a flat shoulder on the large pair separation side of the second peak, are successfully reproduced.

A more sensitive test of our calculations is the prediction of the transverse pair-correlation function in the liquid-vapor interface. We show in Fig. 8 a comparison of the results obtained from the calculations reported in this paper and the experimental data of Flom *et al.* [45,46]. Our calculations reproduce the important finding that the transverse pair-

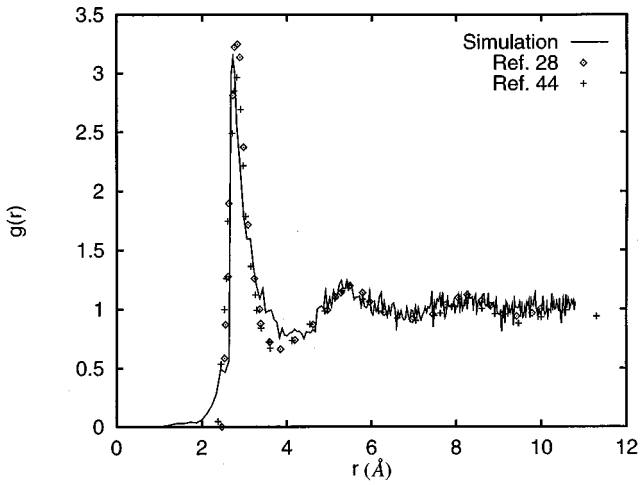

FIG. 7. Calculated pair-correlation function for bulk liquid Ga (solid line), compared with the measured pair-correlation function ($\diamond\,\diamond\,\diamond$, Ref. [28]; $+\,+\,+$, Ref. [44]).

correlation function in the liquid-vapor interface of a metal is essentially the same as that in the bulk liquid, despite the difference in local ion core density and the nonuniform distribution of the ion cores along the normal to the interface.

The most sensitive test of our calculations, and the one of most interest to us, is the prediction of the longitudinal density distribution. The longitudinal density distribution of the ions was obtained from a histogram of the distance between a particle and the center of the mass of the slab; the density profiles in the $+z$ and $-z$ directions were averaged to obtain the reported density distribution. Anticipating the results found, we also have calculated the single-particle density distribution in the plane of the liquid-vapor interface. As shown in Fig. 9, the latter distribution is featureless, despite the fact (to be demonstrated below) that the longitudinal density distribution has damped oscillatory character in the

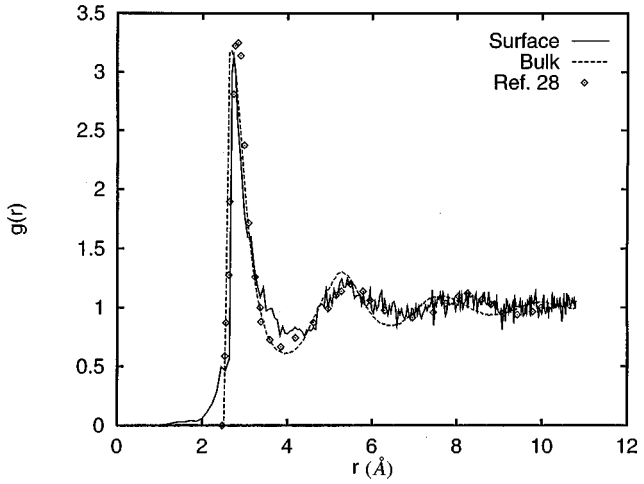

FIG. 8. Transverse pair-correlation function in the liquid-vapor interface of Ga, compared with the measured pair-correlation function in the interface and in the bulk liquid at $T=373$ K and density 0.051 23 atoms/Å^3. The measured pair-correlation functions in the Ga liquid-vapor interface and in bulk Ga have been shown to be the same within experimental error (see Ref. [45]).

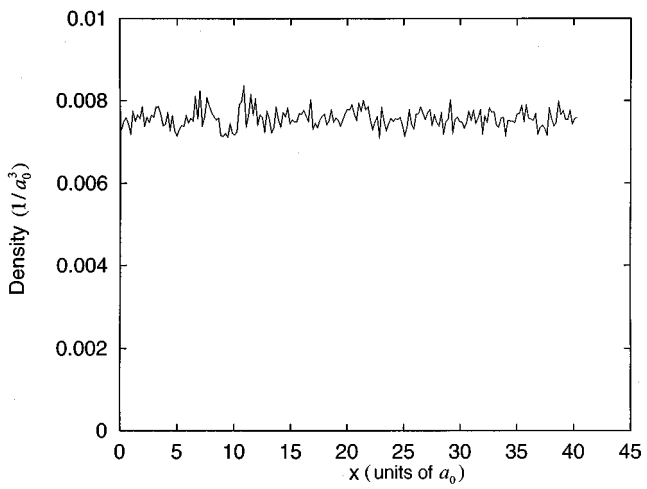

FIG. 9. Transverse singlet density distribution in the liquid-vapor interface of Ga.

liquid-vapor interface, with a maximum density of order 20% larger than the bulk density. In Fig. 10 we compare the calculated longitudinal density distribution in the liquid-vapor interface of Ga with the distribution inferred from x-ray reflectivity measurements by Pershan and co-workers [17–20]. Since the published experimental longitudinal density distribution is given in normalized form, we have normalized our simulation data to make the comparison shown. Clearly, the locations of the peaks in the longitudinal density distribution are well described by the calculations reported, but the amplitude of the predicted first peak and the depth of the first trough are somewhat greater than that observed (see later discussion). The falloff in density at the outermost edge of the experimental longitudinal density distribution is determined by the functional form chosen for the fitting; it is somewhat faster than the corresponding falloff in the simulated longitudinal density distribution. Overall, we argue that the agreement between the calculated and observed longitudinal density distributions is very good. In Fig. 11 we show the calculated longitudinal ion core density distribution together with the calculated longitudinal valence electron den-

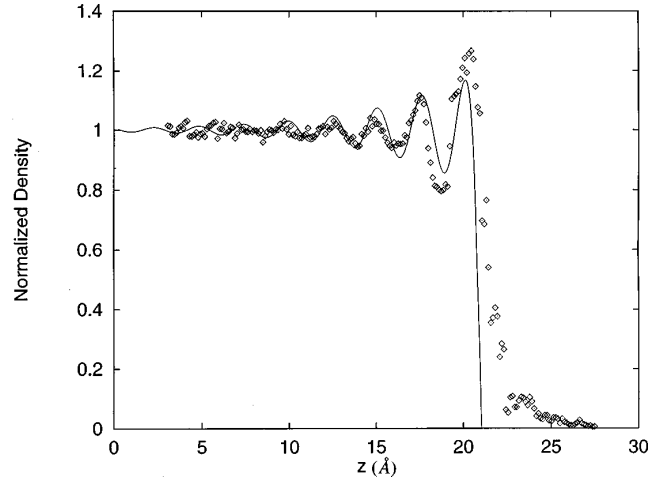

FIG. 10. Calculated ($\diamond\,\diamond\,\diamond$) and observed (—) normalized longitudinal density distributions in the liquid-vapor interface of Ga (experimental data from Ref. [17]).

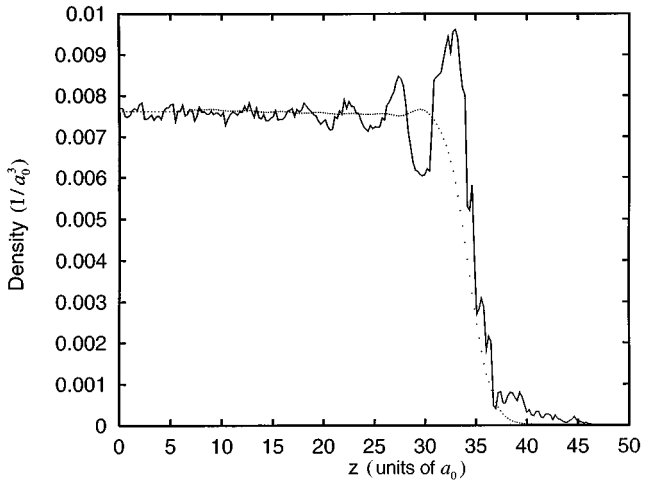

FIG. 11. Longitudinal density distribution in the liquid-vapor interface of Ga (—) and the corresponding electronic density distribution (....).

sity distribution. We note that the outermost peak in the longitudinal valence electron density distribution is essentially coincident with the trough between the first two peaks in the longitudinal ion core density distribution, a consequence of the competition between minimization of the Coulomb interaction, which results from coincidence of the electron and ion core distributions, and the increase in kinetic energy of the valence electrons, which results from the increased electron density gradient required by that coincidence.

The character of the agreement between the observed and calculated longitudinal density distributions deserves careful examination. The observed longitudinal density distribution is certainly partially broadened by long-wavelength thermal excitations (treated as capillary wave excitations in the analysis of the experimental data). Regan *et al.* [47] have shown that the effect of an increase of temperature on the longitudinal density distribution in the liquid-vapor interface of Ga is to decrease the peak heights without changing the peak widths. They successfully account for this observation by representing the mean-square displacement of the nth layer in the form

$$\sigma_n^2 = \mathbf{n}\overline{\sigma^2} + \sigma_0^2 + \frac{k_B T}{2\pi\gamma} \ln\left(\frac{q_{\max}}{q_{\min}}\right), \tag{4.1}$$

where $\overline{\sigma}$ is a measure of the increasing root-mean-square displacement as the density approaches the bulk liquid value and σ_0 is an intrinsic contribution to the root-mean-square displacement; the origin of σ_0 is not identified. The capillary waves that contribute to the mean-square displacement are assumed to have a largest wave vector that is (modπ) the inverse of the ion diameter and a smallest wave vector determined by the experimental resolution. Regan *et al.* obtain an excellent fit to their experimental x-ray reflectivity data with $\overline{\sigma} = 0.393 \pm 0.005$ Å and $\sigma_0 = 0.37 \pm 0.027$ Å.

We interpret the temperature independence of the widths of the peaks in the longitudinal density distribution as follows. The Triezenberg-Zwanzig [48] representation of the surface tension of a pure liquid-vapor interface

$$\gamma = \frac{k_B T}{4} \int_{-\infty}^{\infty} dz_1 \frac{d\rho(z_1)}{dz_1} \int d\mathbf{r}_2 \frac{d\rho(z_2)}{dz_2} (x_2^2 + y_2^2) c(\mathbf{r}_1, \mathbf{r}_2), \tag{4.2}$$

where $c(\mathbf{r}_1, \mathbf{r}_2)$ is the direct correlation function in the liquid-vapor interface, shows that the surface tension has contributions from the entire region over which the gradient of the longitudinal density distribution is nonzero. For the case of Ga, this region extends about four atomic diameters into the bulk liquid. Translated into the language of the macroscopic capillary wave description of surface fluctuations, the ''effective membrane'' that characterizes the liquid-vapor interface must be considered to be a multilayer structure about four atomic diameters thick. We expect that fluctuations of the effective membrane will not affect the spacing and parallelism of these layers since to do so implies creating local variations in the density that increase the free energy. Accepting this picture implies that the capillary wave representation of surface fluctuations is independent of the existence of stratification of the liquid-vapor interface. Since each layer in the interface is distributed about a mean position with a width determined by the same interactions as determine the width of the first peak of the pair-correlation function, we expect both widths to have the same sensitivity to temperature. However, our calculations (see Fig. 6) show that the pair-correlation function of bulk liquid Ga is insensitive to temperature over the range for which x-ray reflectivity data are available and hence so should the widths of the peaks in the longitudinal density distribution.

The amplitude of the first peak in the simulated longitudinal density distribution exceeds that inferred from the fit of the chosen functional form to the experimental reflectivity data by about 10%. This is in the expected direction since the peak amplitude depends on the magnitude of the mean-square displacement [Eq. (4.1)] and the lower limit to the wave vector of the capillary waves that contribute to the observed thermal broadening of the macroscopic sample (estimated to be 0.0064 Å^{-1}) is of the order of 6.6–4.7 times smaller than the smallest-wave-vector thermal excitation that can be supported by the simulation sample (estimated from either the edge length $(40a_0)^{-1} = 0.042$ Å^{-1} or the diagonal length $(56a_0)^{-1} = 0.030$ Å^{-1} of the surface of the simulation sample; see Fig. 9). If, following Regan *et al.* it is assumed that the maximum-wave-vector capillary wave that contributes to the thermal broadening is (modπ) the inverse of the atomic diameter, this difference in smallest wave vectors implies that the contribution of the term $(k_B T/2\pi\gamma)\ln(q_{\max}/q_{\min})$ to the mean-square displacement is smaller for the simulation sample than that for the macroscopic sample used in the experiments by a factor of 1.9–1.5. At 300 K, using the known resolution of the x-ray reflectivity experiments and the values of $\overline{\sigma}$ and σ_0 given in Ref. [47], Eq. (4.1) yields $\sigma_1^2 = 0.779$ Å^2; the corresponding calculation for the simulation sample, using the size of the sample to estimate the smallest contributing wave vector, yields $\sigma_1^2 = 0.549$ or 0.617 Å^2. Then the height of the first peak in the simulated longitudinal density distribution should be larger than that observed by 26% or 18% instead of the 10% we find. We suspect that this discrepancy is a signature of residual inaccuracy of the pseudopotential we have used. We

note that, using this pseudopotential, the amplitude of the first peak in the bulk liquid pair-correlation function is smaller than that observed by about 5%, an error that is in the same direction as inferred for the difference in predicted and observed amplitudes of the first peak in the longitudinal density distribution in the liquid-vapor interface.

ACKNOWLEDGMENTS

This work has been supported by a grant from the National Science Foundation. We thank Professor Peter Pershan for a helpful discussion concerning the temperature dependence of the longitudinal density distribution.

[1] M. P. D'Evelyn and S. A. Rice, Phys. Rev. Lett. **47**, 1844 (1981).
[2] J. S. Rowlinson and B. Widom, *Molecular Theory of Capillarity* (Clarendon, Oxford, 1982).
[3] R. M. Townsend and S. A. Rice, J. Chem. Phys. **94**, 2207 (1991).
[4] D. K. Schwartz, M. L. Schlossman, E. H. Kawamoto, G. J. Kellog, P. S. Pershan, and B. M. Ocko, Phys. Rev. A **41**, 5687 (1990).
[5] A. Gomez and S. A. Rice, J. Chem. Phys. **101**, 8094 (1994).
[6] M. P. D'Evelyn and S. A. Rice, J. Chem. Phys. **78**, 5081 (1983).
[7] M. P. D'Evelyn and S. A. Rice, J. Chem. Phys. **78**, 5225 (1983).
[8] M. P. D'Evelyn and S. A. Rice, Discuss. Faraday Soc. **16**, 71 (1982).
[9] J. G. Harris, J. Gryko, and S. A. Rice, J. Chem. Phys. **87**, 3069 (1987).
[10] J. G. Harris, J. Gryko, and S. A. Rice, J. Stat. Phys. **48**, 1109 (1987).
[11] J. G. Harris and S. A. Rice, J. Chem. Phys. **86**, 5731 (1987).
[12] Z. Cai, J. Harris, and S. A. Rice, J. Chem. Phys. **89**, 2427 (1988).
[13] J. Gryko and S. A. Rice, J. Phys. F **12**, L245 (1982).
[14] J. Gryko and S. A. Rice, J. Non-Cryst. Solids **61-62**, 703 (1984).
[15] J. Gryko and S. A. Rice, J. Chem. Phys. **80**, 6318 (1984).
[16] L. Bosio and M. Oumezine, J. Chem. Phys. **80**, 959 (1984).
[17] O. M. Magnissen, B. M. Ocko, M. J. Regan, L. E. Berman, P. S. Pershan, and M. Deutsch, Phys. Rev. Lett. **74**, 4444 (1995).
[18] M. J. Regan, E. H. Kawamoto, S. Lee, P. S. Pershan, N. Maskil, M. Deutsch, O. M. Magnissen, B. M. Ocko, and L. E. Berman, Phys. Rev. Lett. **75**, 2498 (1995).
[19] M. J. Regan, O. M. Magnissen, E. H. Kawamoto, P. S. Pershan, B. M. Ocko, N. Maskil, M. Deutsch, S. Lee, K. Penanen, and L. E. Berman, J. Non-Cryst. Solids **205-207**, 762 (1996).
[20] M. J. Regan, H. C. Tostmann, P. S. Pershan, O. M. Magnussen, E. DiMasi, B. M. Ocko, and M. Deutsch, Phys. Rev. B **55**, 10 786 (1997).
[21] S. A. Rice, J. Non-Cryst. Solids **205-207**, 755 (1996).
[22] B. N. Thomas, S. W. Barton, F. Novak, and S. A. Rice, J. Chem. Phys. **86**, 1036 (1987).
[23] A. J. Brandley and Z. Krist, Phys. Rev. **91**, 302 (1935).
[24] C. S. Barrett, G. F. Koster, and J. H. Wood, Phys. Rev. **126**, 1037 (1962).
[25] V. Heine, J. Phys. C **1**, 222 (1968).
[26] J. Hafner, *From Hamiltonian to Phase Diagrams* (Springer-Verlag, Berlin, 1987).
[27] P. Ascarelli, Phys. Rev. **143**, 36 (1966).
[28] A. H. Narten, J. Chem. Phys. **56**, 1185 (1972).
[29] D. Weare, J. Phys. C **1**, 210 (1968).
[30] J. Hafner and W. Jank, Phys. Rev. B **42**, 11 530 (1990).
[31] See, for example, G. P. Crawford, R. Stannarius, and J. W. Doane, Phys. Rev. A **44**, 2558 (1991), and references therein.
[32] R. W. Shaw, Jr., Phys. Rev. **174**, 769 (1968).
[33] N. D. Lang, *Solid State Physics*, edited by H. Ehrenreich, F. Seitz, and D. Turnbull (Academic, New York, 1973), Vol. 28, p. 225.
[34] N. H. March, Adv. Phys. **6**, 1 (1957).
[35] D. A. Kirzhnits, Sov. Phys. JETP **5**, 64 (1957).
[36] S. H. Vosko, L. Wilk, and M. Nusair, Can. J. Phys. **58**, 1200 (1980).
[37] D. C. Langreth and M. J. Mehl, Phys. Rev. B **8**, 1809 (1983).
[38] W. Kohn and L. J. Sham, Phys. Rev. A **140**, 1133 (1965).
[39] G. B. Bachelet, D. R. Hamann, and M. Schluter, Phys. Rev. B **26**, 4199 (1982).
[40] R. W. Shaw, Jr., J. Phys. C **2**, 2335 (1969).
[41] C. H. Woo, S. Wang, and M. Matsuura, J. Phys. F **5**, 1836 (1975).
[42] M. Matsuura, C. H. Woo, and S. Wang, J. Phys. F **5**, 1849 (1975).
[43] *Atomic Energy Levels*, Natl. Bur. Stand. (U.S.) Circ. No. 467 (U.S. GPO, Washington, DC, 1952), Vol. II, p. 133.
[44] M. C. Bellissent-Funel, P. Chieux, D. Levesque, and J. J. Weis, Phys. Rev. A **39**, 6310 (1989).
[45] E. B. Flom, Z.-h. Cai, A. Acero, B.-h. Lin, N. Maskil, L. Liu, and S. A. Rice, J. Chem. Phys. **96**, 4743 (1992).
[46] E. B. Flom, M. Li, A. Acero, N. Maskil, and S. A. Rice, Science **260**, 332 (1993).
[47] M. J. Regan, P. S. Pershan, O. M. Magnussen, B. M. Ocko, M. Deutsch, and L. E. Berman, Phys. Rev. B **54**, 9730 (1996).
[48] D. G. Triezenberg and R. W. Zwanzig, Phys. Rev. Lett. **28**, 1183 (1972).